

Published: January 31, 2024

Citation: Gallegos-Duarte, M. and Mendiola-Sántibañez, J., D., 2024. Alterations in Cortical Thickness in Children with Congenital Strabismus and Dissociated Vertical Deviation. Medical Research Archives, [online] 12(1).

<https://doi.org/10.18103/mra.v12i1.4901>

Copyright: © 2024 European Society of Medicine. This is an open-access article distributed under the terms of the Creative Commons Attribution License, which permits unrestricted use, distribution, and reproduction in any medium, provided the original author and source are credited.

DOI:

<https://doi.org/10.18103/mra.v12i1.4901>

ISSN: 2375-1924

RESEARCH ARTICLE

Alterations in Cortical Thickness in Children with Congenital Strabismus and Dissociated Vertical Deviation

Martín Gallegos-Duarte^{1*}, Jorge Domingo Mendiola-Sántibañez²

¹Faculty of Medicine, Autonomous University of Querétaro, Mexico

²Faculty of Engineering, Autonomous University of Querétaro, Mexico

*martin.gallegos@uaq.mx

ABSTRACT

Introduction: Little is known about the morphometric changes that occur in the cerebral cortex of children with congenital strabismus and Dissociated Vertical Deviation (DVD). Mathematical morphology provides the opportunity to discover alterations in cortical thickness.

Objective: Identify and measure differences in cortical thickness in children with congenital strabismus and DVD.

Materials and Methods: Twenty-two MRI brain studies were conducted, each comprising 120 sagittal slices of 1 mm. A cohort of 11 healthy children formed the control group, and a cohort of 11 children with congenital strabismus and Dissociated Vertical Deviation, both in Dissociated Esotropia and Dissociated Exotropia formed the case group. Differences in cortical thickness between both groups were compared and identified using the FreeSurfer suite. Subsequently, areas of interest were analyzed using the ImageJ program to determine density, area, size, and pixel quantity in these regions. Study results are presented through tables and figures.

Results: Twelve inflated brain projections were obtained from 2640 MRI images. Thickness differences between both groups exhibited three areas with significant morphometric changes: the Left Angular Gyrus, Left Supramarginal Gyrus, and Right Pars Opercularis.

Discussion: Children with congenital strabismus and DVD showed changes in cortical thickness that could be identified and measured through Voxel-Based Morphometry (VBM). It is plausible to consider that these changes are related to suppression, aiming to avoid diplopia.

Keywords: VBM, neural substrate, plasticity, congenital strabismus, morphology, Angular Gyrus.

Introduction

Congenital strabismus represents the utmost disruption of the human binocular visual system and affects 3% of the global population¹. Sometimes Congenital strabismus manifests dissociated movements because, in some way, they do not adhere to Hering's law. This law states that the nervous impulse for coordinated eye movement is sent in equal measure to the extraocular muscles. However, dissociated movement is not proportional to this law².

It is known that patients with congenital strabismus are stereoblind and can avoid diplopia by suppressing the superimposed image of the deviated eye and, on the other hand, by decreasing the image quality of the deviated eye, a condition known as amblyopia.

Studies based on fMRI in adults with strabismic amblyopia have not demonstrated the existence of long-range interocular suppression in V1, V2, or V3. On the other hand, studies in primates regarding the cortical representation of areas of cortical suppression during binocular vision suggest that the elimination of diplopia occurs not in V1 but at some unspecified higher cortical level⁴.

Through neuroimaging studies of children with congenital strabismus, morphological and neurofunctional alterations have been identified, revealing failures in cortical integration, suggesting that some oculomotor reflexes go beyond cortical control and, consequently, exacerbate. This happens concurrently with a decrease in some sensory abilities⁵⁻⁷.

Morphometric studies using Voxel-Based Morphometry (VBM) have demonstrated a deficit in connectivity and a decrease in fine

granular elements of cortical white matter in children with congenital strabismus⁸. Additionally, a decrease in gray matter in different areas of the cerebral cortex has been noted⁹, as well as atrophy of cortical gray and white matter¹⁰.

In congenital strabismus, it is possible to evaluate visual information from each eye separately¹¹. It is also possible to precisely identify and measure its sensory and oculomotor manifestations¹². By correlating neuroimaging studies with clinical findings, it has been demonstrated that congenital strabismus has cortical alterations^{5,6,13,14}.

T1-weighted MRI images analyzed through VBM allow the detailed identification of cortical morphometric and neurofunctional changes¹⁵. Various neuroimaging studies have already assessed cortical thickness in different diseases such as ADX¹⁶,

schizophrenia, multiple sclerosis, autism¹⁷, Huntington's disease, Alzheimer's, Parkinson's, cerebral palsy, amblyopia^{9,18}, to identify and measure the most significant changes that occur in the cerebral cortex of patients with these diseases.

The VBM technique has been employed to identify morphometric changes in the cerebral cortex that do not appear in conventional MRI studies but are related to the visual system and strabismus^{6,9,13,19-21}.

To identify cortical thickness in patients with dissociated strabismus, the Free Surfer program was used. This program has a set of automated tools for cortical surface reconstruction from structural magnetic resonance images¹⁶.

The cerebral cortex is a thin layer of highly folded tissue containing a large area of

cortical tissue in the cranial cavity. The sulci of the cerebral cortex are irregular in shape and highly variable among different individuals, both in their configuration and anatomical location. However, Free Surfer's tools solve the folding problem by using flat maps of the cerebral surface, allowing the entire surface to be viewed. The morphological variations of each inflated brain projection for a group of patients result from the heterogeneities of the characteristics of each analyzed patient, once the compensations and automated reconstruction that the Free Surfer suite performs in response to these heterogeneities are made^{23,24}. This allows the evaluation and comparison of cortical thickness differences between individuals and between a case group and a control group²⁵. The program also allows the expansion of the cerebral cortex as if it were a flat map and uses coordinates and distance measurements, enabling the identification of the distribution and location of differences in the cortical surface using specific anatomical references that can be in a schematic model, such as fissures and lobes^{26,27}.

Results obtained through the FreeSurfer suite schematically present the cortical thickness of the case group on a color scale, where yellow represents an increase and blue signifies a decrease in cortical thickness compared to the control group. Meanwhile, gray indicates that there are no statistically significant differences between both groups. Thickness differences are anatomically located in easily identifiable areas on the inflated brain model (Figures 1 and 2).

On the other hand, the ImageJ program is a scientific software for mathematical morphology that allows the processing of images, analysis,

and quantification of obtained data, making it possible to precisely measure the number of pixels, as well as the area they represent in a specific area of interest²⁸.

Patients and Methods.

Patients with congenital strabismus and Dissociated Vertical Deviation (DVD) were selected, both in Dissociated Esotropia (DE) and Dissociated Exotropia (DX). The case group comprised 11 children with congenital strabismus and Dissociated Vertical Deviation, while the control group consisted of 11 healthy children. All patients underwent optometric and ophthalmologic examinations, including determination of visual acuity, refraction, ocular motility, fusion, retinal correspondence, and visual preference. All patients were natives of Querétaro, Mexico, and had no neurological pathology (Table 1).

Table 1.

ID	Case group (n= 11)				
	Sex	Age	Clinical diagnosis	ARC	Suppression
1	Female	11	DX	Yes	Yes
2	Female	11	DX	Yes	Yes
3	Female	9	DX	Yes	Yes
4	Female	10	DX	Yes	Yes
5	Female	11	DE	Yes	Yes
6	Female	11	DX	Yes	Yes
7	Female	11	DX	Yes	Yes
8	Female	7	DX	Yes	Yes
9	Female	11	DX	Yes	Yes
10	Male	8	DX	Yes	Yes
11	Female	11	DE	Yes	Yes

The table displays the clinical characteristics of the patients comprising the case group. All patients presented Dissociated Vertical Deviation, with 9 of them exhibiting exotropia and Dissociated Vertical Deviation (DX), and 2 with esotropia and Dissociated Vertical Deviation (DE). All patients showed suppression and anomalous retinal correspondence (ARC).

For the acquisition, processing, analysis, and interpretation of images, three different tools were employed: i) MRI, ii) FreeSurfer, and iii) ImageJ.

i) Sagittal brain cohorts with a thickness of 1 mm were processed using 3D T1 MRI without contrast medium for each of the 22 brains in the sample. The equipment and protocol had the following specifications: Philips Intera 1.0T System, Version 10.6 FastFeel Echo (FFE) Sequence, weighted to T1 in 3D mode, field of view (FOV) 230 mm, Real FOV (RFOV) 80%, Cohort thickness (Slice Thickness) 1 mm, no gap between cohorts, echo time (TE) 6.9 ms;

repetition time (TR) 25 ms; flip angle (FA) 30 degrees; number of excitations (NAS): 1; number of cohorts: 120.

ii) The MRI studies of both groups were processed and compared using Voxel-Based Morphometry (VBM) with the automated FreeSurfer program to identify regions with significant changes in cortical thickness in the case group (Figures 1 and 2).

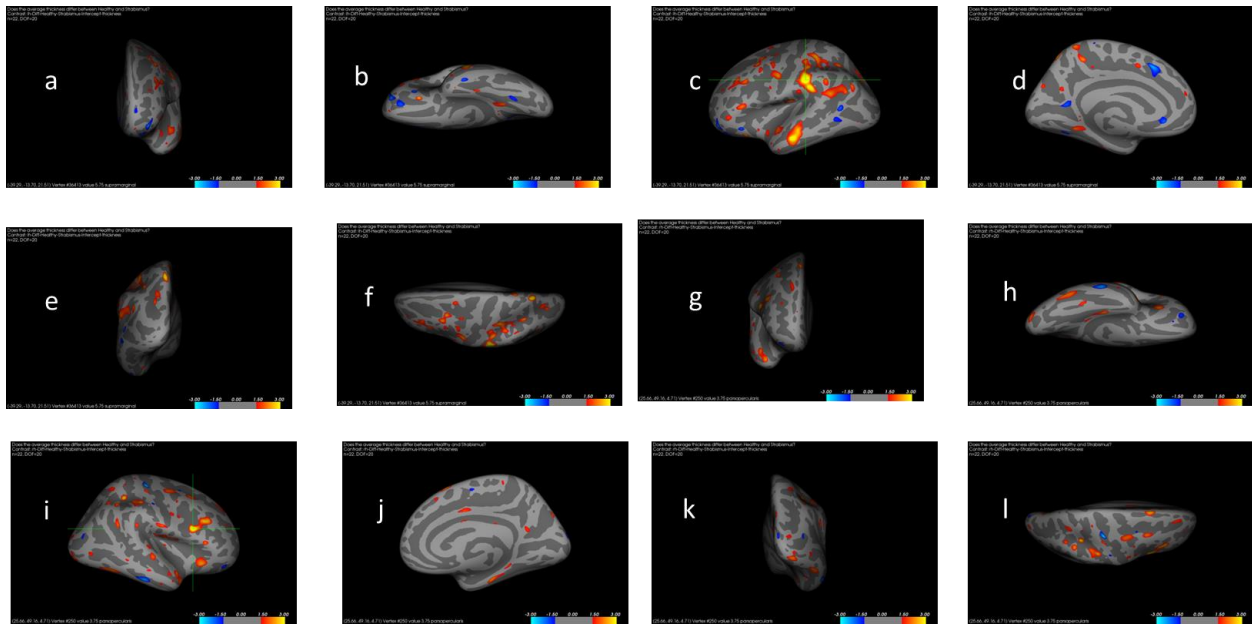


Figure 1. Inflated brain projections obtained using the FreeSurfer suite. The cortical thickness differences between the two analyzed groups are illustrated: a) Anterior Left Hemisphere (LH), b) Inferior LH, c) Lateral LH, d) Medial LH, e) Posterior LH, f) Superior LH, g) Anterior Right Hemisphere (RH), h) Inferior RH, i) Lateral RH, j) Medial RH, k) Posterior RH, l) Superior RH.

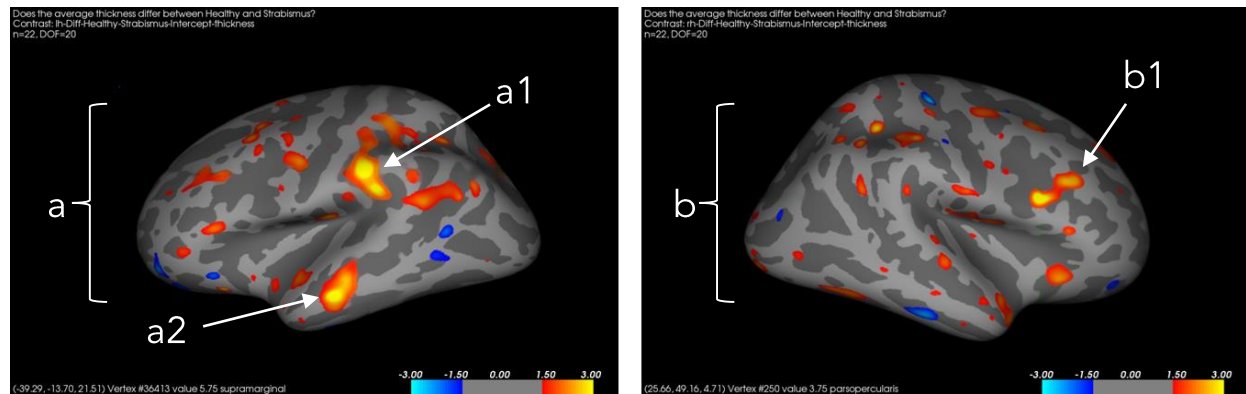


Figure 2. Inflated brain projections. In yellow, a significant increase of 3 mm in cortical thickness is shown in the Angular Gyrus (a1) and the inferior Temporal Gyrus (a2). Meanwhile, in the right hemisphere (b), there is a noteworthy increase in cortical thickness in the Pars Opercularis (b1).

iii) The threshold of each region of interest was measured using the ImageJ program, calculating minimum and maximum values and the quantity of pixels within the color

range that formed the images. The most prominent regions of interest were processed (Figure 3).

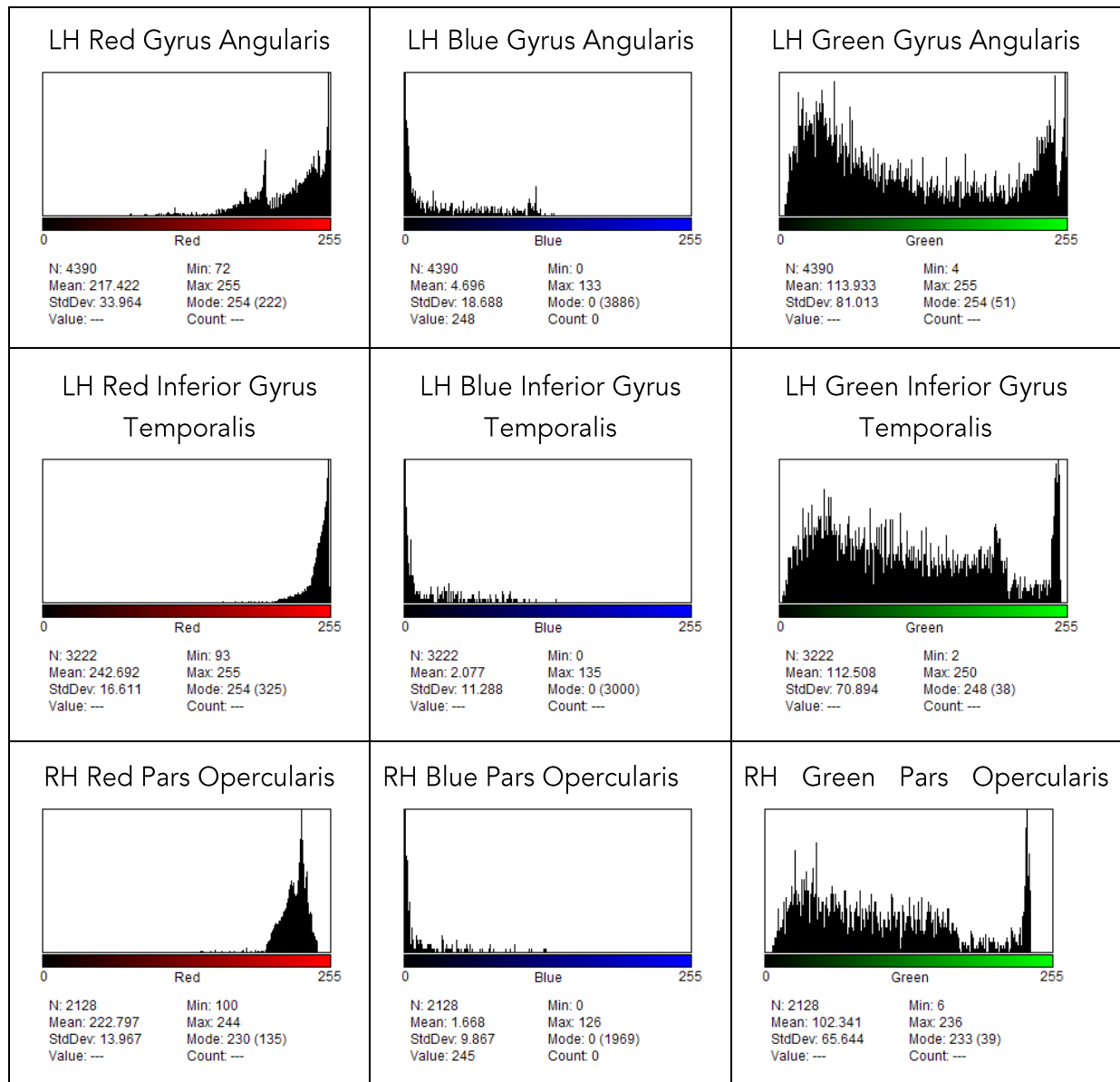


Figure 3. Histograms were created to display the thresholding and weighting of each color constituting the images of the regions of interest. From top to bottom: Left Hemisphere Angular Gyrus, Left Hemisphere Inferior Temporal Gyrus, and Right Hemisphere Pars Opercularis.

Using the ImageJ program, the most notable features of the regions of interest were determined. The anatomical zone was identified, and measurements were taken for area, pixel significance, standard deviation,

perimeter, and solidity (Table 2). This program facilitated the analysis and interpretation of the color bar accompanying the images provided by the FreeSurfer suite (Figure 2).

Table 2.

Pixel values found in the different areas of interest in the case group (n = 11)						
Anatomical Zone	Area	Mean	StdDev	Perim.	Solidity	Function
Gyrus Angularis Left Hemisphere	4390	112.015	32.38	389.886	0.662	Processes and assigns a common code between visual and auditory information
Inferior Gyrus Temporalis Left Hemisphere	3222	119.095	24.671	247.252	0.928	Visual Processamento, Working Memory
Pars Opercularis Right Hemisphere	2128	108.945	23.109	244.693	0.76	It only supports a single stimulus. Semantic, phonological, and syntactic process

The table provides a detailed breakdown of the attributes of each image corresponding to the anatomo-functional zones with the highest cortical thickness found in the problem group.

For a better comprehension of the findings, the color scale was quantified, expressing the

extreme and intermediate values by analyzing the pixels as well, using the ImageJ program. The increase in cortical thickness encompassed colors ranging from red to yellow, i.e., from +1.50 mm to +3.00 mm (Figure 4).


					
Scale	Absolute color in pixels	Perceived Color	Color range	Range in pixels	Range in millimeters
+ 3 mm	255	Yellow	Golden-Yellow	192-225	62.625-3 mm
+ 2.625 mm	191.25	Golden	Amber-Golden	128-191	2.25-2.625 mm
+ 2.25 mm	127.5	Amber	Orange-Amber	64-127	1.875-2.25 mm
+ 1.875 mm	63.75	Orange	Red-Orange	63-126	1.5-1.875 mm
+ 1.5 mm	0	Red	Grey-Red	0-62	0-1.5 mm

Figure 4. The figure displays the pixel composition and its interpretation. Measurements were established using the ImageJ program.

Using the thresholding operator, warm tones were separated from cool tones to determine the quantity of pixels comprising the cortical

thickness changes in each hemisphere (Figures 5 and 6).

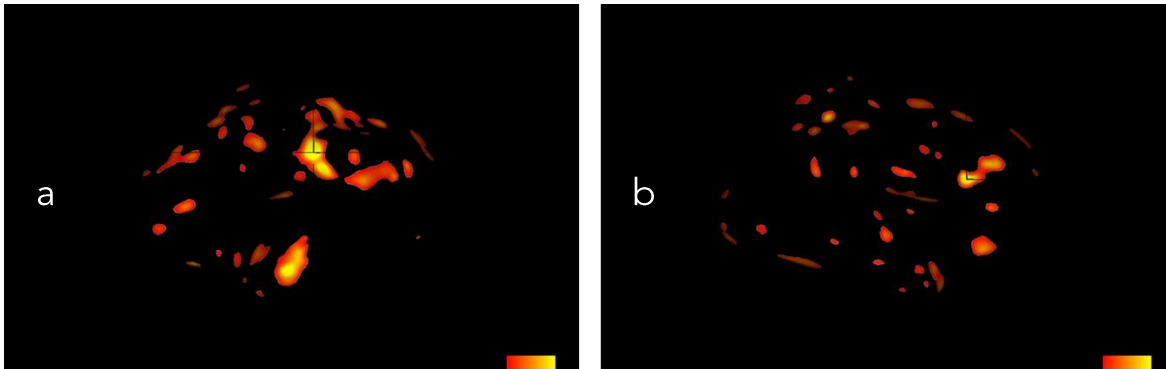


Figure 5 Yellow areas were identified indicating an increase in cortical thickness on the lateral surface of the left hemisphere (a) and the right hemisphere (b) after removing non-significant values. The increase in thickness in different areas signifies a larger affected surface in the left hemisphere compared to the right.

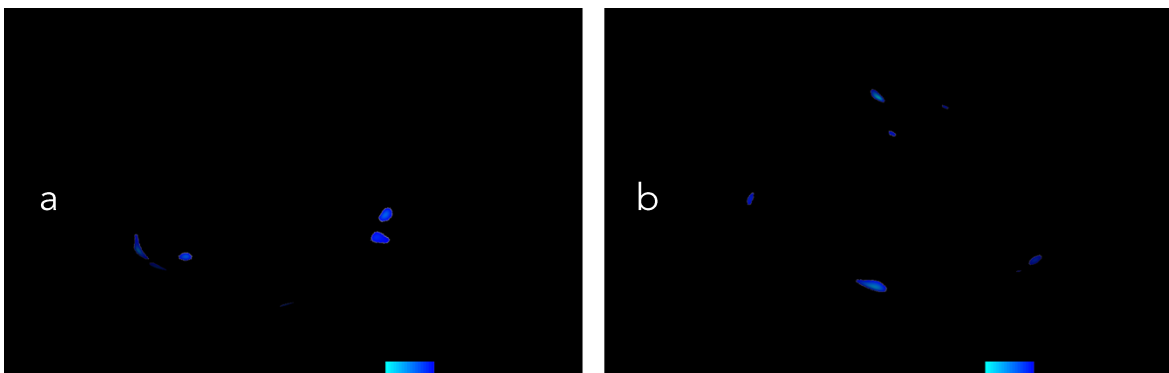


Figure 6 Left hemisphere (a) and right hemisphere (b) of the case group were identified, once non-significant values were removed. The decrease in cortical thickness in the case group was relatively insignificant.

Results

A total of 22 brains were analyzed, and 2640 MRI images were processed for analysis using the FreeSurfer suite, resulting in 12 projections of inflated brain surface map reconstructions (Figure 1).

Three areas showed a significant increase in cortical thickness: the Left Angular Gyrus and Pars Opercularis, as well as the Right Temporal Gyrus (Figure 2, Table 2).

The left hemisphere exhibited the most substantial changes with a larger affected surface (Figure 2a and Figure 5). Upon

detailed analysis of these images using Voxel-Based Morphometry (VBM), differences in pixel density or solidity were identified. The Left Inferior Temporal Gyrus showed the highest density (0.928), while the Left Angular Gyrus represented a larger area (4,390).

The pixel distribution of the Angular Gyrus displayed a predominance of red and yellow with respective transitions, with an absolute value of 112,015 and an area of 4,390, representing the area with the greatest increase in cortical thickness in the left hemisphere. Meanwhile, the Left Inferior

Temporal Gyrus of the same hemisphere showed an absolute value of 119,095 and an area of 3222, representing the second zone of interest with greater cortical thickness in the left hemisphere. On the other hand, the Pars Opercularis was the most prominent area in the right hemisphere with an absolute value of 108,945 and an area of 2128 (Table 2).

A color scale was obtained for the identification of cortical thickness with each of its parameters (Figure 4). Warm-colored areas represented the maximum cortical thickness found in the sample relative to normality (Figure 5), while blue colors indicated areas with the lowest thickness (Figure 6).

Discussion

It has been suggested that changes in cortical thickness in patients with strabismus are indicative of neuroadaptive adjustments to compensate for deficits in visual processing areas, and cortical suppression requires intense neuronal activity, leading to an increase in thickness in certain strategic areas of the cerebral cortex^{19,29}.

The suppression is a skill inherent to congenital strabismus that appears to be driven by neuroadaptive changes, although the precise location remains unclear^{30 31,32 33}. From a sensory standpoint, the visual pathway in patients with congenital strabismus receives simultaneous information from both retinas with a harmonized spatiotemporal frequency. Therefore, the deviated eye projects information with a similar temporal frequency but dissimilar spatial frequency. Despite this, strabismic children do not experience diplopia, and while strictly stereoblind, they can simultaneously perceive

non-corresponding points, i.e., they can fuse the sharp image from the fixing eye with the blurred image from the non-fixating eye through some extrafoveal area, a condition known as Anomalous Retinal Correspondence (ARC), observed in all patients in the case group (Table 1).

The Voxel-Based Morphometry (VBM) results in this study reveal an increase in thickness in specific cortical areas in children with congenital strabismus. An increase in cortical thickness was identified in the supramarginal gyrus and the Angular Gyrus, which is contiguous and represents a secondary extension of the visual association pathway. The primary function of this pathway is to process and assign a common code for visual and auditory information.

While the color scale accompanying the images allowed for a qualitative assessment by observers (Figure 2), a quantitative mathematical basis was required for this research to quantify the degree of morphological alteration in the regions of interest. This determination was necessary to establish the area and pixel volume for statistical purposes, as demonstrated in the histograms (Figure 3, Table 2). In evaluating the changes, consideration was given not only to the increase in cortical thickness but also to the area, pixel density, strategic location in the cerebral cortex, and their possible clinical correlation (Table 2).

It is possible that these changes are related to the clinical findings of the patients, including ocular deviation and dissociated movement from a motor perspective, and suppression and ARC from a sensory perspective.

Conclusions

It is plausible to consider that the increased thickness in the Angular Gyrus and supramarginal gyrus of the left hemisphere and the Pars Opercularis of the right hemisphere represents a neuroadaptive response that somehow promotes suppression, aiming to prevent visual confusion and diplopia in patients with congenital strabismus and Dissociated Vertical Deviation.

Conflicts of Interest Statement:

None

Acknowledgements Statement:

None

Funding Statement:

None

Bibliography:

1. Engle EC. Genetic basis of congenital strabismus. *Archives of ophthalmology*. 2007; 125(2):189.
2. Bridgeman: The Theory of Binocular Vision: Ewald... - Google Académico. Accessed November 6, 2023. https://scholar.google.com/scholar_lookup?title=The%20Theory%20of%20Binocular%20Vision%3A%20Ewald%20Hering%20%281868%29&author=B%20Bridgeman&author=L%20Stark&publication_year=1977&book=The%20Theory%20of%20Binocular%20Vision%3A%20Ewald%20Hering%20%281868%29
3. Thompson B, Maehara G, Goddard E, Farivar R, Mansouri B, Hess RF. Long-Range Interocular Suppression in Adults with Strabismic Amblyopia: A Pilot fMRI Study. *Vision*. 2019;3(1):2. doi:10.3390/vision3010002
4. Economides JR, Adams DL, Horton JC. Interocular Suppression in Primary Visual Cortex in Strabismus. *J Neurosci*. 2021;41(25):5522-5533. doi:10.1523/JNEUROSCI.0044-21.2021
5. Mechelli A, Crinion JT, Long S, et al. Dissociating reading processes on the basis of neuronal interactions. *Journal of cognitive neuroscience*. 2005;17(11):1753-1765.
6. Gallegos-Duarte M M. Dissociated Vertical Divergence. *Strabismus*. 2012;20(1):31-32. doi:10.3109/09273972.2011.651769
7. ten Tusscher MPM. Dissociated Deviation in the Infantile Strabismus Syndrome. *Strabismus*. 2012;20(1):33-34. doi:10.3109/09273972.2011.650816
8. Mendiola Santibañez MSJ, Gallegos-Duarte M, Ortiz-Retana JJ, López-Campos CE. Segmentación y análisis granulométrico de sustancia blanca y gris en IRM para el estudio del estrabismo usando transformaciones morfológicas. 2007;28(2):92-104.
9. Mendola JD, Conner IP, Roy A, et al. Voxel-based analysis of MRI detects abnormal visual cortex in children and adults with amblyopia. *Human Brain Mapping*. 2005;25(2):222-236. doi:10.1002/hbm.20109
10. Ouyang J, Yang L, Huang X, et al. The atrophy of white and gray matter volume in patients with comitant strabismus: Evidence from a voxel-based morphometry study. *Mol Med Rep*. 2017;16(3):3276-3282. doi:10.3892/mmr.2017.7006
11. Gallegos-Duarte M. *Comportamiento de la coherencia bioeléctrica cortical en el estrabismo congénito*. Tesis Doctoral. Universidad Autónoma de Querétaro; 2017. <https://docplayer.es/59017501-Comportamiento-de-la-coherencia-bioelectrica-cortical-en-el-estrabismo-congenito.html>>COMPORTAMIENTO DE LA COHERENCIA BIOELÉCTRICA CORTICAL EN EL ESTRABISMO CONGÉNITO</div><div><iframe frameborder="0" style="border-bottom: 2px solid #eee; border-top: 0px; scrolling="no" src="http://docplayer.es/docview/68/59017501/" width="728" height="946" allowfullscreen></iframe></div></div>
12. Bagolini B. Objective evaluation of sensorial and sensorimotorial status in esotropia: their importance in surgical prognosis. *British Journal of Ophthalmology*. 1985;69(10):725-728. doi:10.1136/bjo.69.10.725
13. Brodsky MC. The Role of Cortical Alterations in Infantile Strabismus. *Strabismus*. 2012;20(1):35-36. doi:10.3109/09273972.2011.650817

14. Gallegos-Duarte M MS, JJ OR, Rubin de Celis-Monteverde B, Vidal-Pineda R, Sigala-Zamora A. Dissociated deviation. A strabismus of cortical origin. *Cir Cir.* 2007; 75(4):237-243.
15. Höflich A, Ganger S, Tik M, et al. Imaging the neuroplastic effects of ketamine with VBM and the necessity of placebo control. *NeuroImage.* 2017;147:198-203. doi:10.1016/j.neuroimage.2016.12.032
16. Almeida Montes LG, Prado Alcantara H, Martinez Garcia RB, De La Torre LB, Avila Acosta D, Gallegos-Duarte M. Brain Cortical Thickness in ADX: Age, Sex, and Clinical Correlations. *Journal of Attention Disorders.* 2013;17(8):641-654. doi:10.1177/1087054711434351
17. McAlonan GM. Mapping the brain in autism. A voxel-based MRI study of volumetric differences and intercorrelations in autism. *Brain.* 2004; 128(2):268-276. doi:10.1093/brain/awh332
18. Duan Y, Norcia AM, Yeatman JD, Mezer A. The Structural Properties of Major White Matter Tracts in Strabismic Amblyopia. *Invest Ophthalmol Vis Sci.* 2015;56(9):5152-5160. doi:10.1167/iovs.15-17097
19. Chan S tak, Tang K wing, Lam K cheung, Chan L kong, Mendola JD, Kwong KK. Neuroanatomy of adult strabismus: a voxel-based morphometric analysis of magnetic resonance structural scans. *NeuroImage.* 2004;22(2):986-994. doi:10.1016/j.neuroimage.2004.02.021
20. Hagmann P, Cammoun L, Gigandet X, et al. Mapping the Structural Core of Human Cerebral Cortex. *PLOS Biology.* 2008; 6(7):e159. doi:10.1371/journal.pbio.0060159
21. Horton J, Hocking D. An adult-like pattern of ocular dominance columns in striate cortex of newborn monkeys prior to visual experience. *J Neurosci.* 1996;16(5):1791-1807. doi:10.1523/JNEUROSCI.16-05-01791.1996
22. Sabbah N, Sanda N, Authié CN, et al. Reorganization of early visual cortex functional connectivity following selective peripheral and central visual loss. *Sci Rep.* 2017;7(1):43223. doi:10.1038/srep43223
23. Dale AM, Fischl B, Sereno MI. Cortical Surface-Based Analysis. *NeuroImage.* 1999;9(2):179-194. doi:10.1006/nimg.1998.0395
24. Reuter M, Schmansky NJ, Rosas HD, Fischl B. Within-subject template estimation for unbiased longitudinal image analysis. *NeuroImage.* 2012;61(4):1402-1418. doi:10.1016/j.neuroimage.2012.02.084
25. Pagnozzi AM, Fripp J, Rose SE. Quantifying deep grey matter atrophy using automated segmentation approaches: A systematic review of structural MRI studies. *NeuroImage.* 2019;201:116018. doi:10.1016/j.neuroimage.2019.116018
26. Fischl B, Dale AM. Measuring the thickness of the human cerebral cortex from magnetic resonance images. *Proceedings of the National Academy of Sciences.* 2000;97(20):11050-11055.
27. Fischl B, Sereno MI, Dale AM. Cortical Surface-Based Analysis. *NeuroImage.* 1999;9(2):195-207. doi:10.1006/nimg.1998.0396
28. Abramoff, M.D, Magalhaes, P.J, Ram, S.J. Image Processing with ImageJ. *Biophotonics International.* 2004;11(7):36-42.
29. Yan X, Lin X, Wang Q, et al. Dorsal Visual Pathway Changes in Patients with Comitant

- Extropia. Yang S, ed. *PLoS ONE*. 2010;5(6): e10931. doi:10.1371/journal.pone.0010931
30. Gallegos-Duarte M. Regarding Noise and Visual Confusion. *EC Neurology*. 2016; 4(2):46-47.
31. Harrad R, Sengpiel F, Blakemore C. Physiology of suppression in strabismic amblyopia. *Br J Ophthalmol*. 1996;80(4):373-377.
32. Kohler PJ, Meredith WJ, Norcia AM. Revisiting the functional significance of binocular cues for perceiving motion-in-depth. *Nat Commun*. 2018;9(1):3511. doi:10.1038/s41467-018-05918-7
33. Ondategui Parra JC, Borrás García R, Pacheco Cutillas M. *Visión binocular*. Universitat Politècnica de Catalunya; 1998. Accessed September 13, 2016. <http://public.ebib.com/choice/PublicFullRecord.aspx?p=4310074>
34. Bock EA, Fesi JD, Baillet S, Mendola JD. Tagged MEG measures binocular rivalry in a cortical network that predicts alternation rate. Price NSC, ed. *PLoS ONE*. 2019;14(7):e0218529. doi:10.1371/journal.pone.0218529
35. Molnar-Szakacs I, Iacoboni M, Koski L, Mazziotta JC. Functional Segregation within Pars Opercularis of the Inferior Frontal Gyrus: Evidence from fMRI Studies of Imitation and Action Observation. *Cerebral Cortex*. 2005;15(7):986-994. doi:10.1093/cercor/bhh199